Nonlinear dynamic simulation and control of large-scale reheating furnace operations using a zone method based model

Yukun Hu [a*], CK Tan [b], Jonathan Broughton [c], Paul Alun Roach [b], Liz Varga [a]

[a] Complex Systems Research Centre, School of Management, Cranfield University, Bedford MK43 0AL, UK
[b] Faculty of Computing, Engineering and Science, University of South Wales, Pontypridd CF37 1DL, UK
[c] British Steel R&D Swinden Technology Centre, South Yorkshire S60 3AR, UK

Abstract

Modern reheating furnaces are complex nonlinear dynamic systems having heat transfer performances which may be greatly influenced by operating conditions such as stock material properties, furnace scheduling and throughput rate. Commonly, each furnace is equipped with a tailored model predictive control system to ensure consistent heated product quality such as final discharge temperature and temperature uniformity within the stock pieces. Those furnace models normally perform well for a designed operating condition but cannot usually cope with a variety of transient furnace operations such as non-uniform batch scheduling and production delay from downstream processes. Under these conditions, manual interventions that rely on past experience are often used to assist the process until the next stable furnace operation has been attained. Therefore, more advanced furnace control systems are useful to meet the challenge of adapting to those circumstances whilst also being able to predict the dynamic thermal behaviour of the furnace. In view of the above, this paper describes in detail an episode of actual transient furnace operation, and demonstrates a nonlinear dynamic simulation of this furnace operation using a zone method based model with a self-adapting predictive control scheme. The proposed furnace model was found to be capable of dynamically responding to the changes that occurred in the furnace operation, achieving about ±10 °C discrepancies with respect to measured discharge temperature, and the self-adapting predictive control scheme is shown to outperform the existing scheme used for furnace control in terms of stability and fuel consumption (fuel saving of about 6%).

Keywords: zone method; reheating furnace; hybrid model; nonlinear dynamic simulation; self-adapting predictive control

1. Introduction

In every hot-rolling operation, the reheating furnace is a critical component determining quality of end-product: steel blooms, billets or slabs (known as stock). Therefore, most reheating processes require precise control of the stock temperature and temperature uniformity over the entire heating period. Whilst energy consumption in a reheating furnace depends greatly on production conditions such as stock dimension, material grade and throughput, improved control of the furnace firing pattern can lead to indirect energy saving through improving the furnace set-point temperatures. However, the multi-zone cascaded construction of reheating furnaces and the associated thermal inertia of the furnace make the task of furnace temperature control very challenging, particularly on occasions of

[*] Corresponding author. Tel.: +44 (0)24 765 22333; E-mail address: yukun.hu@cranfield.ac.uk; ceykhu@gamail.com (Y. Hu)

changes in, for example, target reheating temperature, production rate and/or stock dimension and material grade, and production delay.

With the advent of more affordable computing power, the use of model-based control in steel reheating furnaces has become widespread since the 1970s [1]. Currently three categories of furnace models may be distinguished. First, Computational Fluid Dynamics (CFD) models, a class of models that is based on physical laws related to the fluid flow, mixing, combustion and heat transfer which must be solved on a densely discretized computational domain of the real furnace detailed geometry. They have relatively high accuracy but at the expense of being computationally intensive. Due to the movement of the stocks inside the furnace as well as the charging and discharging process, the transport phenomena are periodically transient. *Prieler et al.* [2,3] simulated the movement of the stock in a virtual way; the furnace geometry including stock does not change, and the thermal energy contained in a stock is moved from one position to the next. To overcome the issue of high processing time in CFD simulation, *Casal et al.* [4] and *Mayr et al.* [5] developed a method for the simulation of reheating furnaces in steady-state, in which the stocks are modelled as a highly viscous fluid. Although low calculation time can be achieved, compared to transient or iterative approaches, relatively this method only applies to periodic transient reheating operation. Therefore, CFD models are unsuitable for simulating the thermal behaviour of transient steel reheating in real or near real-time with varying stock geometry and non-uniform batch scheduling. The second class is semi-empirical models [6–10], which do not rigidly adhere to specific physical laws but which may rely on measured data as model inputs. They aim to achieve extremely fast simulations but have to compromise on accuracy. These models are often used for supervisory temperature control, which relies mainly on a limited number of thermocouple measurements installed along the furnace roof and hearth. Given that these limited thermocouple measurements cannot fully represent the temperature map over large control zones within the furnace, and that their responses are not always representative of the temperature in a control zone, this approach can cause inconsistencies in temperature regulation. Consequently, the supervisory temperature control has to compromise on inherent inaccuracies in both measurements and modelling assumptions. The situation can be further exacerbated by unsteady heating demands since highly dynamic thermal behaviours exist within the furnace that can only be captured by thermocouple measurements with time delay. The third class, ‘black-box’ models, do not involve any specific physical law but may commonly contain sets of adaptive weights, i.e. numerical parameters that are tuned by a learning algorithm with training data. These models are capable of approximating non-linear functions of their inputs, and include the class of statistical models known as Artificial Neural Networks (ANNs) [11–13]. However, in practice the application of this kind of models is limited by the availability of training data.

Alternatively, mathematical models based on the zone-method [14] are widely employed for industrial furnaces [15]. The advantages of a zone model lie in its ability to represent radiation heat transfer accurately within high temperature furnace enclosures with far less discretization requirements for the computational domain. The fluid flow, mixing and heat release from combustion of fuel may be derived separately from other sources thus making the overall computation process much more efficient. Zone method based models (so-called zone models) belong to this category. *Emadi et al* [16] investigated the heating characteristics of stocks in a walking beam reheating furnace using a simplified zone model. They used an empirical correlation to calculate the convective coefficient on

the stock's surfaces, thereby avoiding the need to calculate for enthalpy exchange due to flows of combustion products; a simple model was used to estimate radiation flux on the stock's lateral faces rather than calculating any interactive radiation between all faces of the stocks. *Tan et al.* [17] developed a three-dimensional furnace model to simulate the thermal performances of a large-scale reheating furnace. The modelling approach takes into account the net radiation interchanges between the top and bottom firing sections of the furnace and also allows for enthalpy exchange due to the flows of combustion products between these sections. *Hu et al.* [18,19] combined the advantages of the classical zone method of radiation analysis and conventional CFD in a robust manner which overcame the challenges of incorporating three-dimensional flow field within the zone model and considering interactive radiation between stocks. The model was developed based on first-principles and verified by the trial data from the same reheating furnace as modelled. With all model parameters fixed, simulations were repeated with different time-step setting. Results suggest that the virtual furnace model was able to predict the overall thermal behaviour of the furnace with reasonable accuracy. Even with consumer-level PC hardware, the developed model showed a fairly promising computational efficiency, about 170 times faster than the actual run time of large-scale reheating furnaces, so that it was then successfully incorporated into population based genetic algorithm for multi-objective optimisation of reheating furnace operations [20]. Their work also suggests that the developed model is capable of capturing the nonlinear dynamic of the furnace and has great potential to be incorporated directly into dedicated furnace control algorithms. To the best of the authors' knowledge, the literature contains no examples of a model that can perform nonlinear dynamic simulation of walking-beam type reheating furnace operations while also incorporating detailed radiation heat transfer due to the movement of stock in a time-varying computational domain.

The scope of the current paper is thus concerned with the development of a new method for the simulation of nonlinear dynamic operations of reheating furnaces. This novel approach applies the zone method based model [19] together with a self-adapting predictive control scheme, while further taking into account the two-dimensional temperature distribution within the different sections of each stock across its length. An episode of actual furnace operation data, supplied by British Steel, is used to test the model response to the simulated operating conditions in which sufficiently severe transient operating conditions, due to furnace batch scheduling and production delay, were encountered. This paper is organised as follows; Section 2 details the scope for simulation of furnace operations; Section 3 presents the virtual furnace model and the control strategy used in the nonlinear dynamic simulation; Section 4 offers results and analysis of the simulated furnace operation described in Section 2; finally, in Section 5 conclusions in relation to this overall study are drawn with clearly outlined suggestions for future exploitation of the developed model.

2. Scope for simulation of furnace operations

The furnace studied is a large-scale walking-beam bloom reheating furnace (130 t/h), which has an effective length of 36 m and width of 10 m. The furnace height varies between 4.0 m and 4.7 m along the length of the furnace, illustrated in Figure 1. In total 71 burners are installed within 6 control zones (CZ), and CZs 2 and 4 are slaves to CZs 1 and 3 respectively. The thermal inputs of the slave control zones are set implicitly in proportion to the thermal inputs of the master control zones. Blooms are charged into the furnace at one side, move through the furnace while being heated, and are discharged at the opposite side.

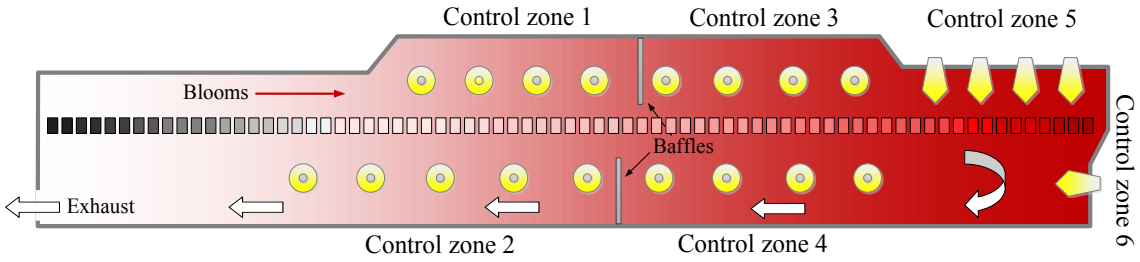

Figure 1. Outline of the reheating furnace under steady state operation

2.1 Existing control solution

The existing process control solution for the reheating furnace is shown in Figure 2. The control utilises a calibrated reheating model based on a 2-dimensional finite difference heat conduction model for calculating the temperature distributions of the blooms as they pass through the furnace. The heat flux on the surfaces of individual blooms is determined from the knowledge of the furnace temperatures and bloom positions which in turn are obtained through communication with the Supervisory Control and Data Acquisition (SCADA) [21] and Material Tracking System (MTS), respectively. A forward prediction of the final discharge temperature distribution is made using the reheating model, the current zonal temperature set-points, and the zonal temperature increase/decrease capabilities of the furnace. This information is subsequently transformed into a new set of furnace set-points, at every model's iteration, which is then used to regulate the burner heat input accordingly. The change of set-point is a self-adapting process. The set-points used to control the furnace temperature in the current instance are adjusted by the reheating model in the previous instance, and are readjusted at every time interval.

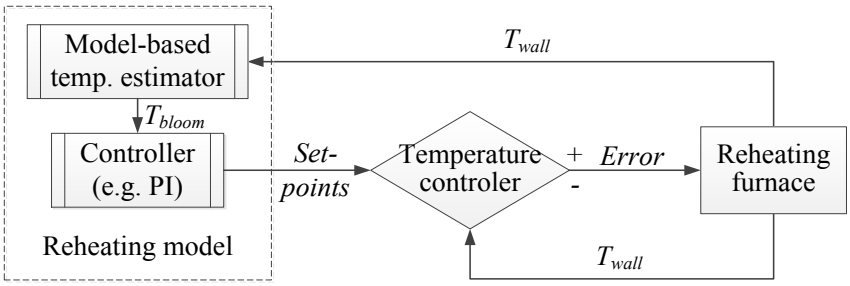

Figure 2. Existing process control solution for the reheating furnace

In this control solution, the new furnace set-points are often determined by comparing the desired and predicted bloom temperature profiles. However, the desired bloom temperature profile depends on designed operating conditions under steady state and that profile is rarely published. Therefore, there are still technical challenges posed by highly dynamic operation of reheating furnaces in practice. An example of such a challenge is the problem of improving set-point temperatures in real time while maintaining continuous production as far as possible without under- or over-heating the discharged bloom due to an unplanned disturbance.

2.2 Operating conditions

Previously, British Steel had conducted experiments in which the temperature field near the soak zone (control zone 5) was obtained from an advanced radiometric imaging camera. The data acquisition period for the experiment spans about 45 hours, during which two different batches of mild steel blooms (so-called SB1 and SB2) were processed by the rolling mills. Their dimensions and mass are summarized in Table 1. The real-time dimension history of the charged blooms, including length and height to width ratio, is shown in Figure 3(a). Steel batches SB1 and SB2 were to be heated to mean bulk temperature of 1250 °C and 1220 °C respectively. During the whole duration of operation, the furnace production rates were highly non-steady and together with varying stock spacing (as shown in Figure 3(b)), had resulted in the total number of blooms contained in the furnace to vary from about 33 to 96 (as shown in Figure 3(c)). The main challenge in applying the zone model in such a highly dynamic situation was the need to pre-calculate all the radiation exchange factors (a total of 640 sets) for the entire test duration. An improved Monte Carlo ray tracing algorithm [22] was used to perform the pre-calculation of the radiation exchange factors of the computational domain including all faces of stocks. Figure 4 shows representative instants of bloom arrangement within the reheating furnace.

Table 1. Bloom dimensions encountered during furnace operation

Batch no.	Width, m	Height, m	Length, m	Weight, kg
SB1	0.230	0.283	7.028 – 9.409	3568 – 4777
SB2	0.305	0.355	7.521 – 7.625	6352 – 6440

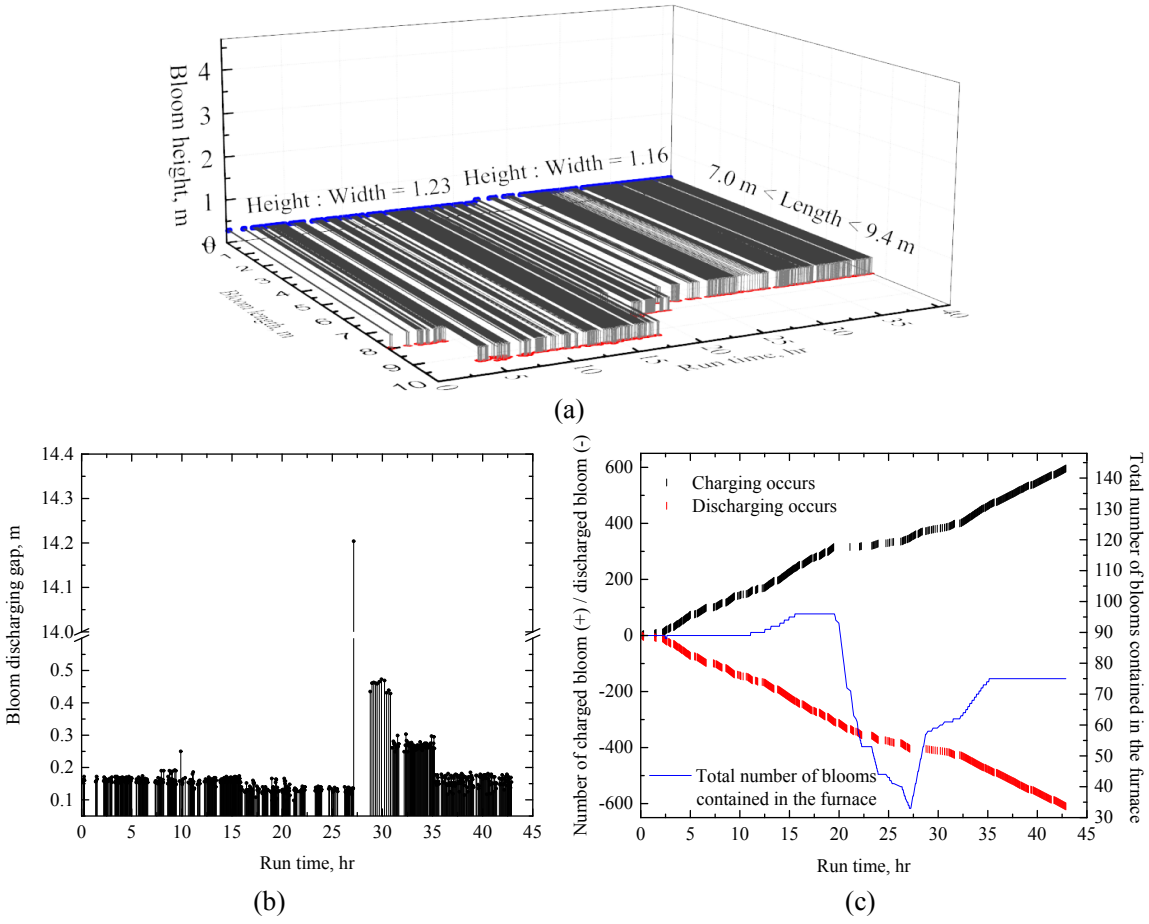

Figure 3. Nonlinear dynamic operating conditions of the reheating furnace: (a) real time dimension history of the charged bloom in the operation; (b) gaps between consecutively discharged blooms; (c) bloom charging and discharging histories

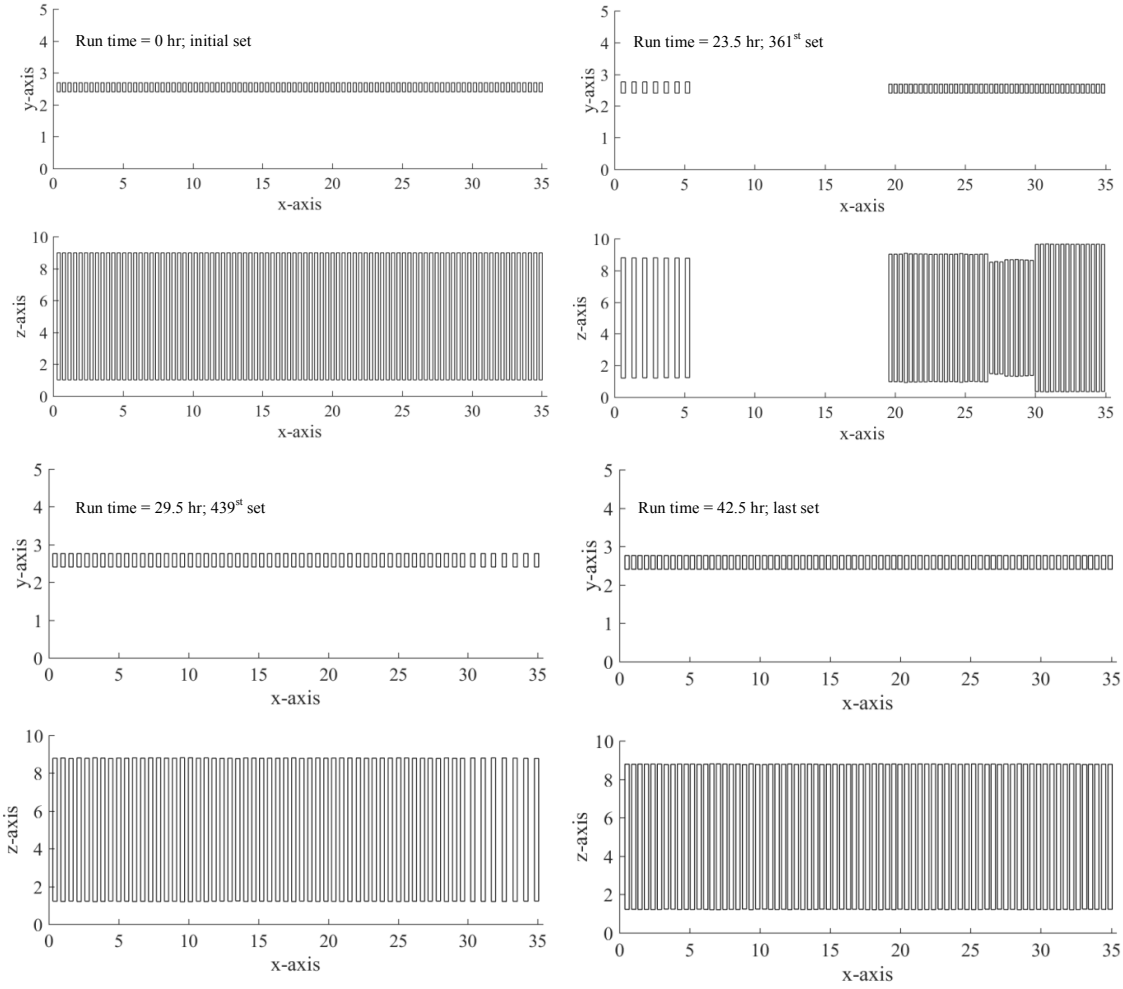

Figure 4. Representative instants of bloom arrangement within the reheating furnace (in scale)

3. Simulation methodology

To establish initial boundary conditions, the virtual furnace model was run from cold start-up until the furnace refractory was well soaked so that it represented a typical thermal condition of the furnace that has been operating for a prolong period of time. In order to facilitate simulation of the dynamic operating conditions, the radiation exchange areas [23] for each instance of bloom distribution (in total 640 instances) with respect to time are pre-calculated and stored for post-processing. This would allow the zone model to retrieve this information 'on-the-fly' during dynamic simulation.

3.1 Overview of the virtual furnace model

The virtual furnace model was developed using the zone method of radiation analysis, namely the zone model. In accordance with the zone method, the furnace was split into 16 sections (across its

length) × 3 sections (across its height) × 6 sections (across its width); in total there are 288 volume zones and 356 surface zones (including 324 surface zones for furnace walls, 32 surface zones for baffle walls, as shown in Figure 5 (in scale with Figure 1). The surface zones for bloom surfaces vary with the number of blooms in the furnace. For example, initially there are 89 blooms in the furnace, which account for 2314 surface zones in total. Each bloom was further split into 6 sections across its length according to the splitting lines on furnace width, so that each bloom was represented by a total of 26 surface zones. This allows the virtual furnace model to investigate variation of temperature along the length of the blooms within the furnace. An energy balance is formulated for each zone considering radiation interchange between all surface and volume zones, the enthalpy transport, source terms associated with the flow of combustion products and their heat release due to combustion [23].

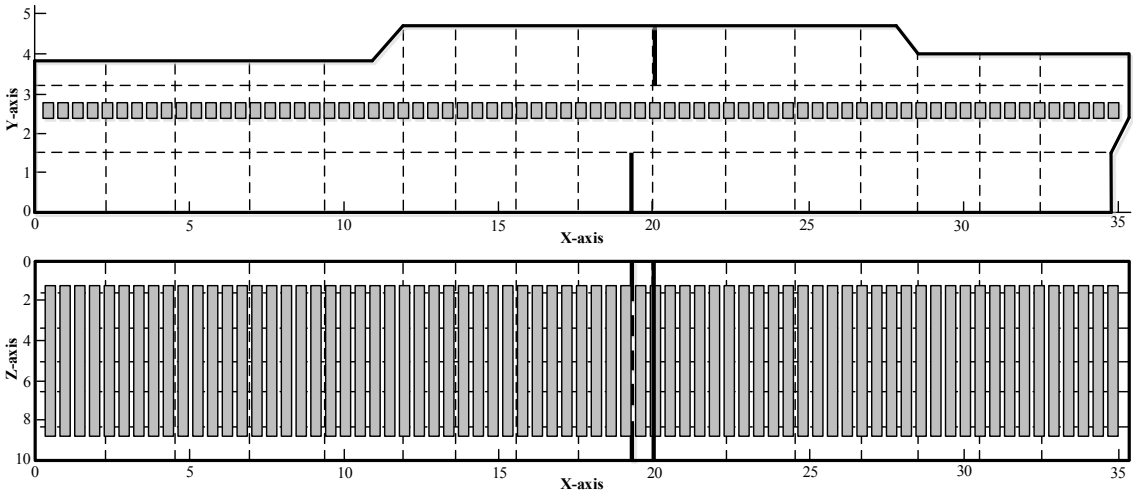

Figure 5. Zoning arrangement in the virtual furnace model

The radiation term in the energy balance equations is written in terms of exchange factors known as directed flux areas (denoted by $\overleftarrow{G_iG_j}, \overleftarrow{G_iS_j}, \overleftarrow{S_iG_j}, \overleftarrow{S_iS_j}$ for gas-gas, gas-surface, surface-gas, and surface-surface exchange respectively in Eq. 1 and 2); these allow for the effects of surface emissivity and the non-grey behaviour of the radiant interchange within the furnace enclosure. The energy balances on all zones yield a set of simultaneous non-linear equations which can be solved to determine the temperature and heat flux at each zone. The time-dependent internal node temperatures of blooms and wall lining can also be calculated by incorporating a transient conduction model. For a system of N volume zones and M surface zones, the following energy balances can be written.

For the i-th volume (gas) zone:

$$\sum_{j=1}^{N} \overleftarrow{G_iG_j}\sigma T_{g,j}^4 + \sum_{j=1}^{M} (1 - A_d/A_j)\overleftarrow{G_iS_j}\sigma T_{s,j}^4 - 4\sum_{n=1}^{n_g} a_{g,n}k_{g,n}V_i\sigma T_{g,i}^4 - (\dot{Q}_{conv})_i + (\dot{Q}_{fuel,net})_i + (\dot{Q}_a)_i + (\dot{Q}_{enth})_i - (\dot{Q}_{wc})_i = 0. \quad \text{(Eq. 1)}$$

Likewise, for the i-th surface zone:

$$\sum_{j=1}^{M}(1-A_d/A_j)\overline{S_iS_j}\sigma T_{s,j}^4+\sum_{j=1}^{N}\overline{S_iG_j}\sigma T_{g,j}^4-A_i\varepsilon_i\sigma T_{s,i}^4+A_i\left(\dot{q}_{conv}\right)_i=\dot{Q}_{s,i} \quad \text{(Eq. 2)}$$

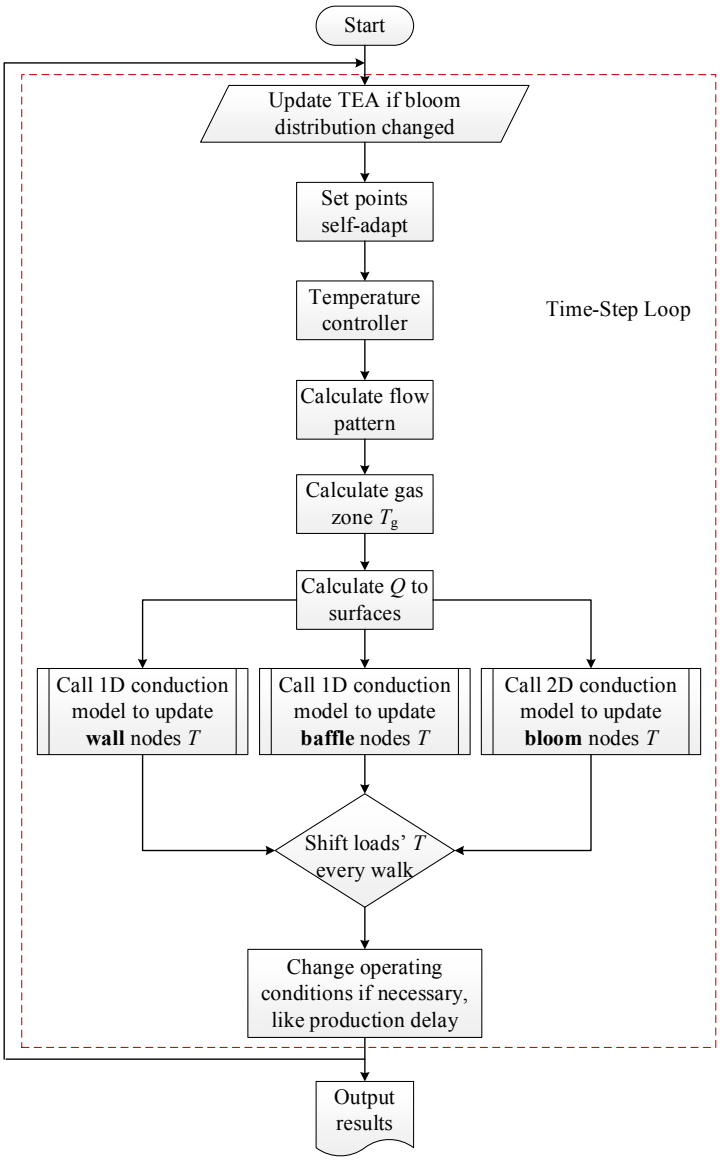

Figure 6. Program flow-chart of the nonlinear dynamic simulation using zone model

Figure 6 shows the program flow-chart of the nonlinear dynamic simulation using the zone model. First, from a given initial boundary condition, including bloom distribution and set-point temperatures, the temperature control and the flow pattern modules are executed sequentially to generate the current flow field. Then, the volume-zone energy balance equations (Eq. 1) are solved using the Newton-Raphson method [24], to yield the gas-zone temperatures (T_g). The calculated gas-zone temperatures are then substituted into the surface-zone energy balance equations (Eq. 2) to determine the rate of heat transfer to each surface zone corresponding to the blooms and furnace wall lining. The temperature distributions within the blooms and wall lining can then be updated by means of a finite

difference conduction analysis. The effect of continuous transport of blooms on their temperature-distance history along the furnace was simulated by a series of discrete pushes at fixed time intervals. At each push, one bloom is discharged, and the positions of all remaining blooms (together with their nodal temperatures) within the furnace are shifted forward towards the discharge end. The first bloom position at the charge end is then substituted with a new bloom at ambient temperature. Operating conditions can also be changed at a specific point in time if necessary, such as production rate and burner fuel flow rates. At the end of each time-step the bloom distribution is checked, and the total exchange area (TEA) will be updated at the beginning of next time-step if the distribution changed. Then, the quadratic flow pattern model re-calculates the flow field inferred by new burner fuel flow rates which are modulated by the temperature controller. The whole procedure can then be repeated sequentially over a series of time steps to predict the nonlinear dynamic furnace operation. For details of TEA and flow pattern calculations, see the references [19,22].

3.2 Control solution used in the simulation

In the actual heating process, there are changing batch, production delay and other measurable disturbances. Proportional–Integral–Derivative (PID) is the standard process controller used in steel reheating furnaces [25]. The PID based feedback compensation to firing rates only applies to steady state operations with fixed set-point temperatures, but cannot correctly respond to these measurable disturbances with large inertia and lag problems. The energy flow in the reheating furnace is unidirectional, and the interaction between the control zones is unilateral. Therefore, the furnace can be considered as a system consisting of *n* cascaded control zones, as shown in Figure 7.

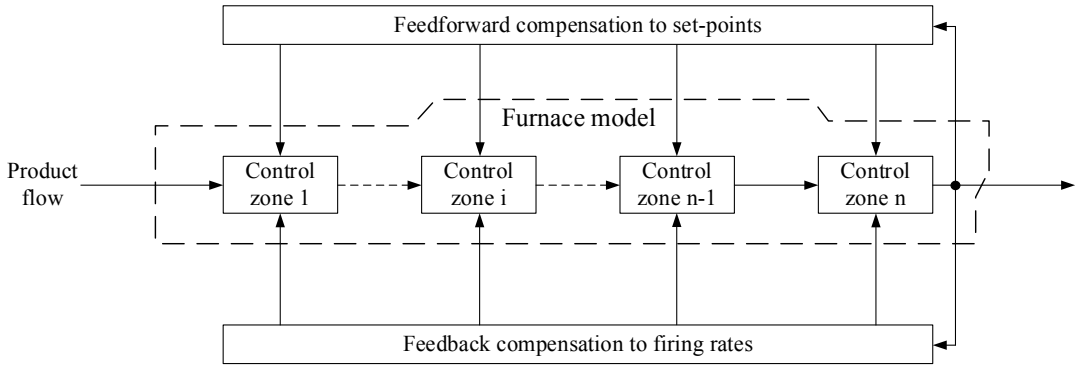

Figure 7. Control solution using in the simulation

Although set-point data of the actual furnace operation are available, they are not reasonably applicable in other furnace models since they relate to a particular process control system. Therefore, a self-adapting predictive control strategy is also applied within the simulation, as shown in Figure 8. The control strategy consists of two control loops: (1) a PID controller in a feedforward loop to compensate for the set-point in each control zone; (2) a normalized PID controller in a feedback loop to compensate for firing rate in each control zone. The former is used to tune set-point temperatures to eliminate measurable disturbances, while the latter is used to regulate burner firing rate to achieve the set-point temperatures and compensate for unmeasurable disturbances. The authors note that the novelties of research reported in the paper is to demonstrate model predictive self-adapting predictive furnace set-point temperature as input to the PID controller. The PID controller in the proposed

control strategy may be replaced by any other type of controller, but this is beyond the scope of this paper.

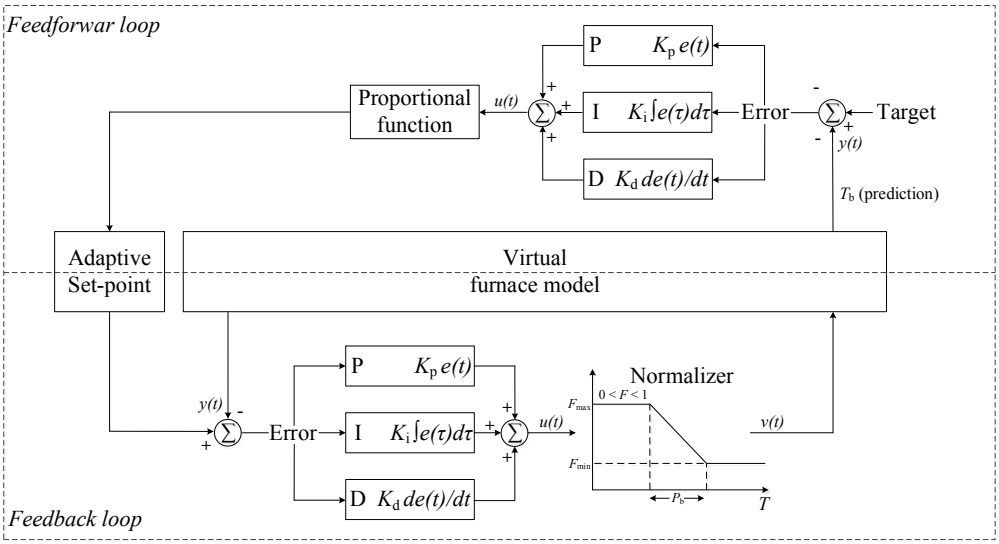

Figure 8. Control strategy used in the nonlinear dynamic simulation

In the feedforward loop, the set-points in a current instance were adjusted based on the comparison of the next time-step discharge temperature (mean bulk temperature of the last bloom) in the virtual furnace model with the target discharge temperature. A standard PID algorithm was implemented where the output $u(t)$ is calculated by summing the proportional, integral, and derivative terms such that:

$$u(t) = K_{\mathrm{p}}e(t) + K_{\mathrm{i}}\int_0^t e(t)dt + K_{\mathrm{d}}\frac{d}{dt}e(t), \qquad \text{(Eq. 3)}$$

where K_{p}, K_{i} and K_{d} denote the proportional, integral and derivative gains respectively, and $e(t)$ is the error, i.e. the difference between target and discharge temperatures in each control zone. In Eq. 3, $u(t)$ represents the required temperature compensation relative to the target temperature at the current time-step and this is then used to predict the discharge temperature of the next time-step. If the discharge temperature of the next time-step is higher than the target temperature, the set-point of heating zones in a future instance is lowered proportionally, and vice versa.

In the feedback loop, $u(t)$ represents the required temperature compensation relative to the set-point temperature (T_{sp}) at the current time-step and this is then used to adjust the burner fuel flow rate (i.e. normalized firing rate v(t) between 0 and 1) in the beginning of the next time-step as defined in Eq. 4.

$$v(t+dt) = v(t) + \frac{F_{\max} - F_{\min}}{P_{\mathrm{b}}}\left(T_{\mathrm{sp}} - u(t)\right), \qquad \text{(Eq. 4)}$$

The overall block diagram of the temperature controller is illustrated in Figure 8. Here $F_{\max}$ and $F_{\min}$ are respectively the normalized (between 0 and 1) maximum and minimum firing rates of the burners, as required by the format of fuel input to the zone model. In the current study, the controller parameters in Fig. 8 have been tuned so that K_{p} = 0.05, K_{i} = 0.5, K_{d} = 0.5 and P_{b} = 200. The authors

note that when applying PID control to a different process, these parameters need to be retuned for better steady-state and dynamic performance.

4. Results and analysis

A snapshot view from the radiometric imaging camera is shown in Figure 9 (Colour figure available online, the same hereinafter; see Appendix for the data of the selected areas). The output images from the camera have been partitioned so that they match directly the zone arrangement of the virtual furnace model. The comparisons between the temperatures predicted by the virtual furnace model and those recorded by the camera show that the maximum local error is less than 50 °C (compared with measured average value). Furthermore, the temperature distribution of the last bloom is not symmetrical as expected. This is due to the opposite firing at the bloom right-hand end (BloomR) being lower than the bloom left-hand end (BloomL). This dynamic feature was also captured by the furnace model, and that should be the result of incorporating the dynamic furnace flow pattern [19]. It implies that the furnace model is capable of correctly representing the temperature distribution within the furnace.

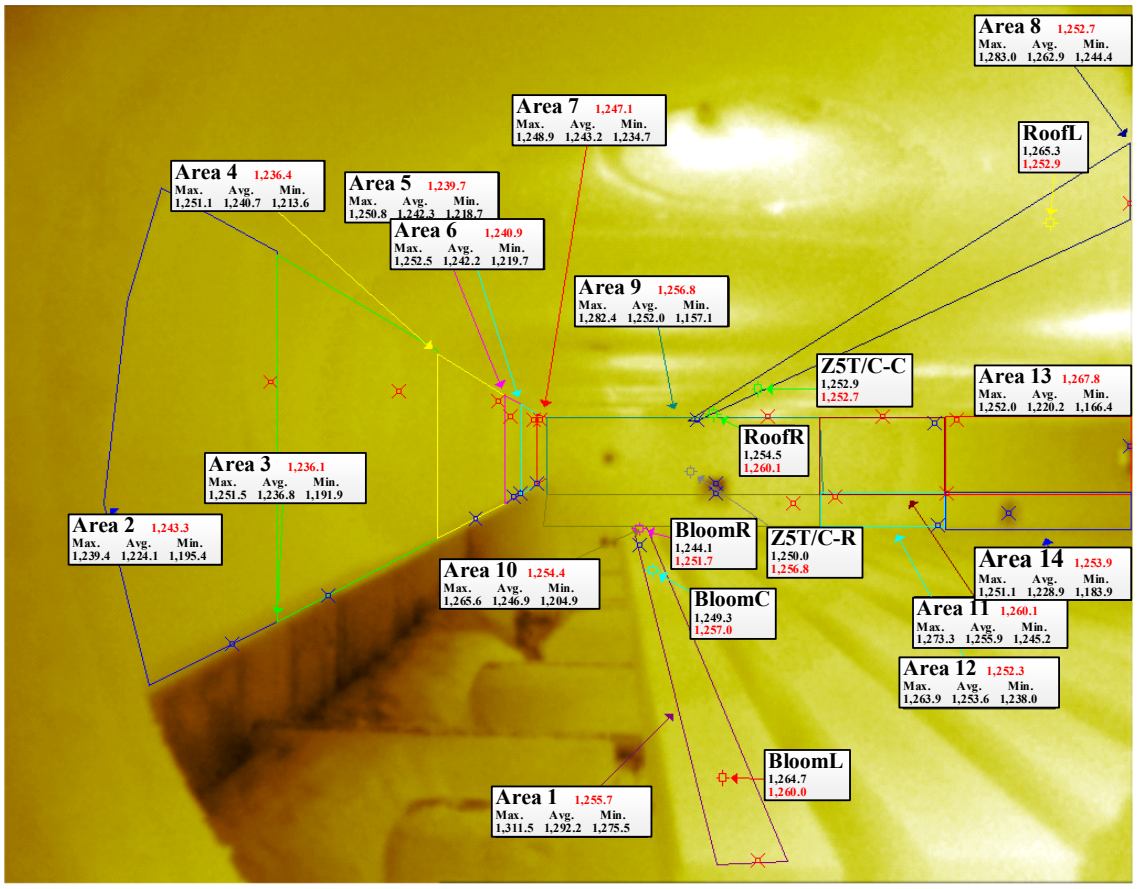

Figure 9. Snap shot of temperature field around soak zone (°C; prediction in red; measurement in black)

In the trial, the actual furnace operational data recorded the measured temperature history of wall areas within the furnace during the dynamic operation. It includes two operation periods in which the

blooms were heated to 1250 °C and 1220 °C respectively. The temperature histories predicted by the model for top and bottom surfaces of the discharged bloom compared well, in general, with actual measurements as illustrated in Figure 10, with discrepancies of about ±10 °C with respect to actual measurements. The larger fluctuations observed in the measured data might be due to the characteristic response of the radiometric thermal imaging camera, when compared to a more idealised response from the zone model. Nevertheless, it is clear that the model can respond to changes in discharging temperature correctly, with discrepancies of about ±5 °C with respect to the target temperature. The discrepancies are considered to be in a reasonable range, and they have no noticeable negative impact on the production process.

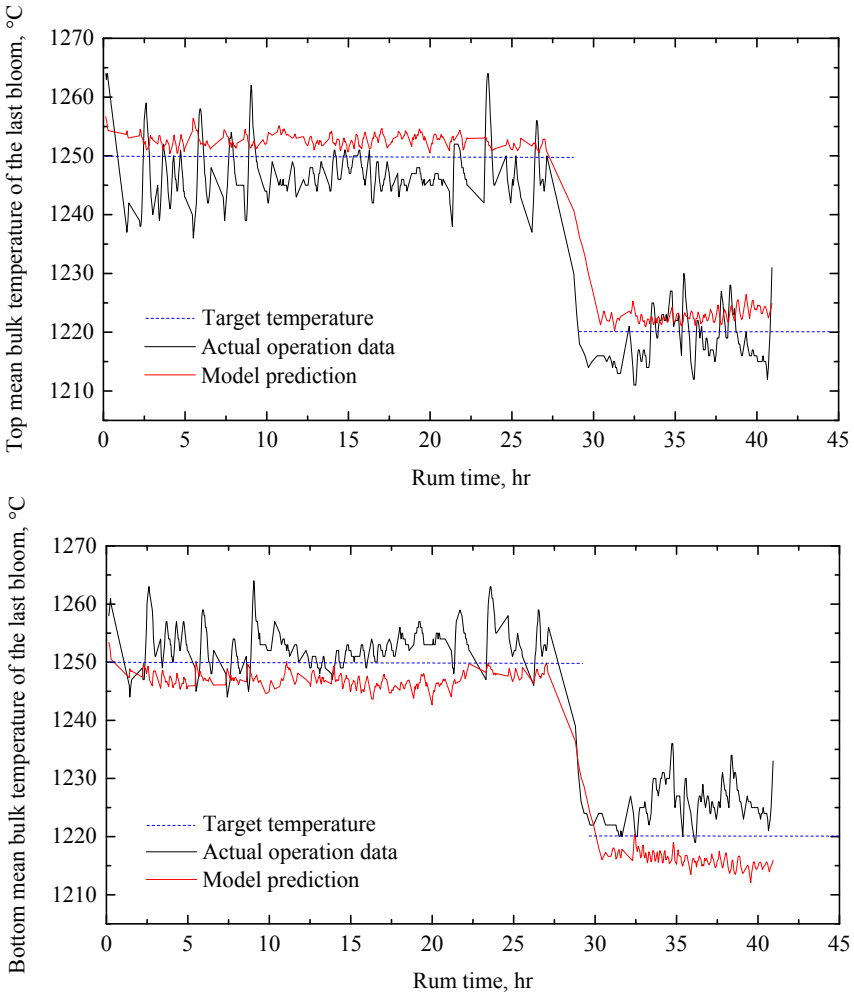

Figure 10. Temperature histories of top and bottom surface of the last bloom

Predicted temperature histories of the furnace walls (discharging-end wall (16, 3, 3, f1*), roof wall (16, 3, 6, f3), and side wall (16, 3, 6, f2)) are also compared with corresponding measurements, as illustrated in Figure 11. The predicted temperature history agreed well, in general, with the

* Face 1 of furnace volume zone located at 16th section in *X* direction, 3rd section in *Y* direction, and 3rd section in *Z* direction [19].

measurements, and their trends are consistent with the temperature history of the last bloom in the dynamic operation.

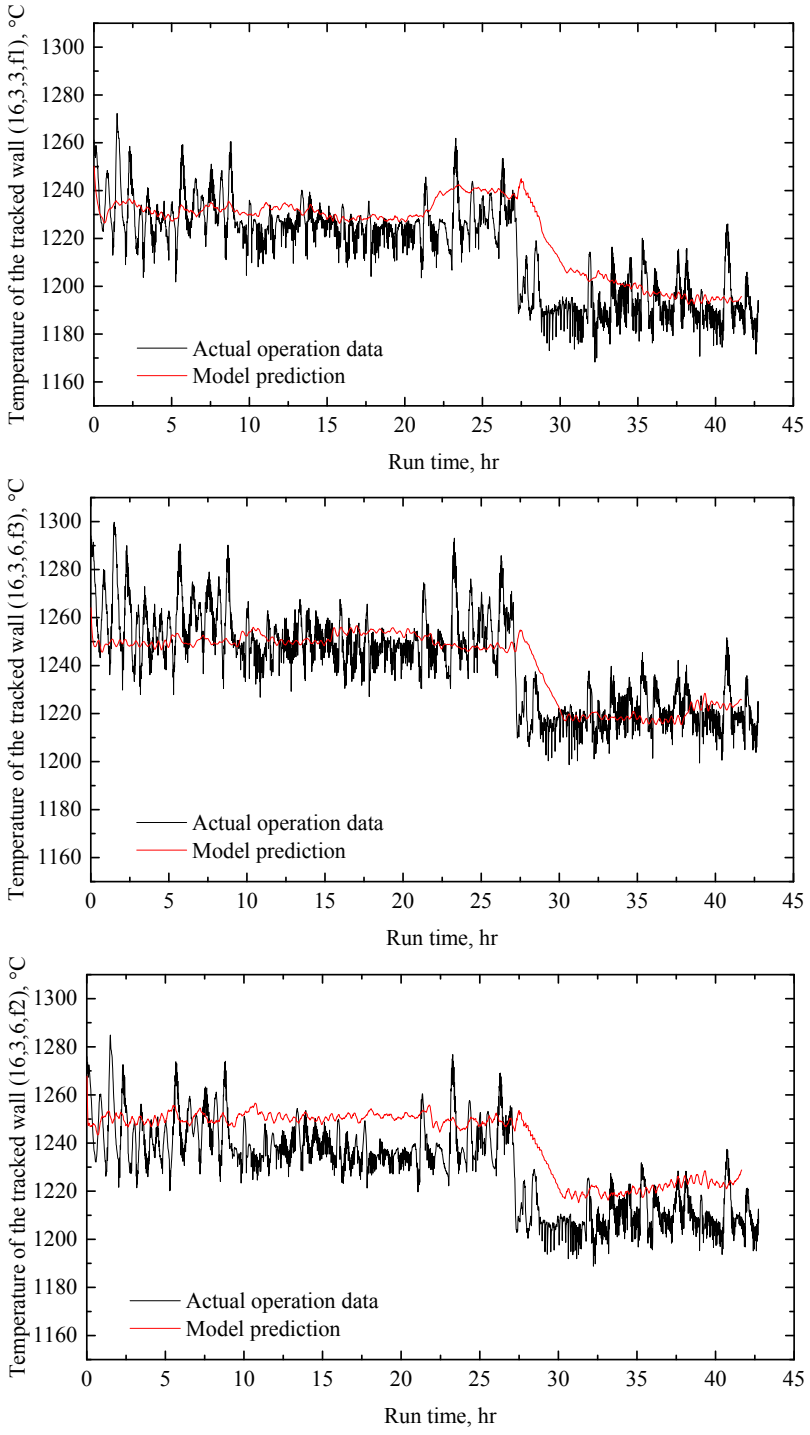

Figure 11. Temperature history of the tracked furnace walls

The simulation results shown in Figure 10 and Figure 11 also suggest that the furnace operation with zone model based control solution was running more stably than that with the existing control solution theoretically. Although the simulated furnace operation is highly dynamic, the zone model based control solution can maintain continuous production as far as possible without any appreciable

overshoot. Figure 12(a) shows the actual set-point temperatures and controlled wall temperatures during the simulated furnace operation. The actual set-point temperatures fluctuated greatly in time and space, especially in control zone 1, and as a result the actual controlled wall temperatures almost synchronize with the set-points during the simulation. The strong fluctuation in the set-point temperatures might be due to the fact that the existing control solution still relies on temperature measurement and cannot capture every dynamic feature caused by heating lag during furnace operations. In contrast, energy balance is inherently encapsulated within the zone model, thus the control solution is able to maintain the furnace wall temperatures with minimal fluctuation, as shown in Figure 12(b). The results imply that the zone model, if employed, is likely to outperform the existing reheating model in responding to dynamic operations and predicting set-point temperatures.

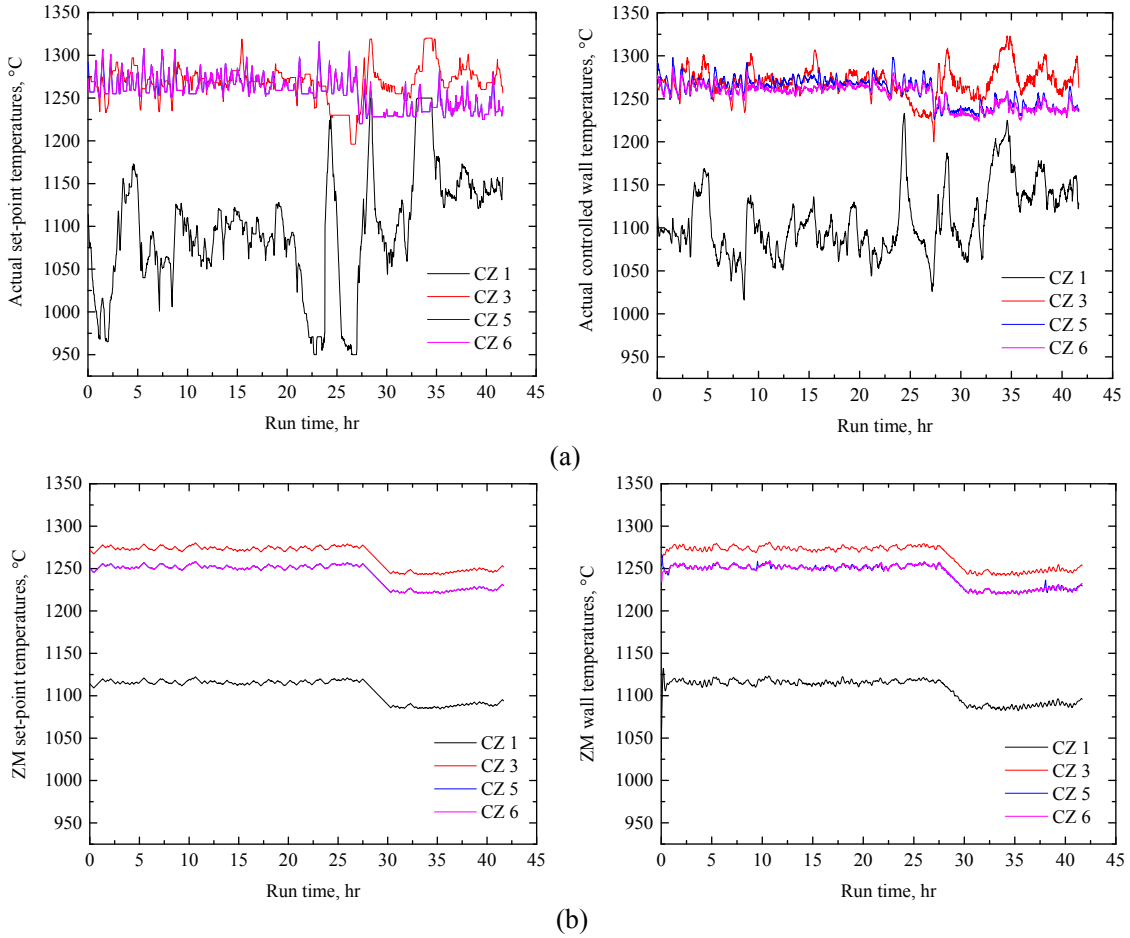

Figure 12. Set-point temperatures and controlled wall temperatures in actual (a, top row) and during the simulated furnace operation (b, bottom row)

During simulation of the operation period, the cumulative thermal energy entering the furnace was also calculated and this was compared with the actual energy consumption (5446 GJ) over the duration of the simulation. The zone model combined with the self-adapting predictive control scheme can achieve a fuel saving of about 6%. This result can be explained through the analysis of the firing rate at each control zone. Figure 13 shows the comparison of firing rates at different control zones in actual operation and zone modelling. In general, the simulated firing rates are considerably more stable than those of the actual ones at most instances. That means the zone model can better

predict the temperature distribution when changes in operation are encountered and the control system can exert a moderate signal to change the furnace set-point temperatures whenever necessary.

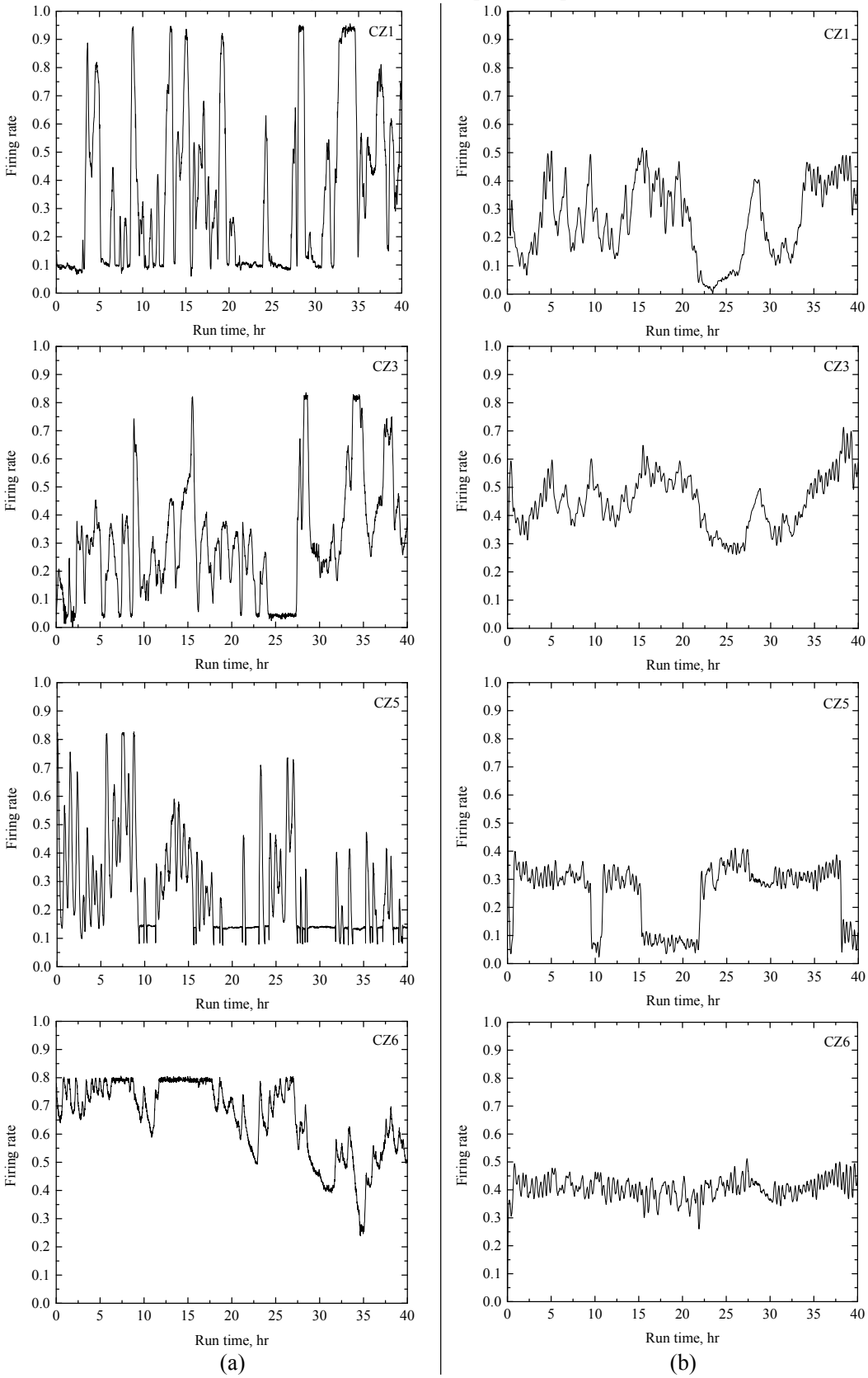

Figure 13. Comparison of firing rate at different control zones in actual (a, left column) and zone modelling (b, right column)

5. Conclusions

This paper presents the application of a zone method based furnace model to simulate a range of dynamic operating conditions in an actual furnace operation. Under a feedback and feedforward combined self-adapting predictive control scheme, detailed radiation heat transfer was calculated in a time-varying computational domain. Compared with the experimental data, in general, the discharged-temperature histories predicted by the model compared well with actual measurements, with discrepancies of about ±10 °C. The furnace model incorporating self-adapting predictive control strategy was found to be capable of adjusting the furnace set-point temperatures dynamically in response to changes in operation, in which non-uniform batch scheduling and production delay were encountered. The simulation results imply that the developed furnace model adopting the proposed self-adapting control scheme would outperform the existing reheating model in responding to dynamic furnace operations and predicting set-point temperatures. If employed, a fuel saving of about 6% can be achieved. This study also suggests that the developed furnace model could be used to understand and improve the operation of modern reheating furnaces.

Acknowledgements

This work was supported by the Research Fund for Coal and Steel (RFCS, DYNAMO RFS-PR-10018) and the Engineering and Physical Sciences Research Council (EPSRC, EP/P004636/1, UK). The first author would like to thank the financial support by National Natural Science Foundation of China (61573381).

Nomenclature

Abbreviations

ANNs	Artificial Neural Networks
CFD	Computational Fluid Dynamics
CZ	Control Zone
MTS	Material Tracking System
PID	Proportional–Integral–Derivative
SCADA	Supervisory Control and Data Acquisition
SB	Steel Blooms
TEA	Total Exchange Area

Symbols

$a_{g,n,}$	weighting coefficient in mixed grey gas model	-
A_d	area of furnace door	m^2
A_i	area of the i-th surface zone	m^2
A_j	area of the j-th door occupied surface zone	m^2
e	error	°C
f	furnace wall numbering	-
F_{max}	proportion of maximum firing rate	-
F_{min}	proportion of minimum firing rate	-

$\overline{G_iG_j}$, $\overline{G_iS_j}$, $\overline{S_iG_j}$, $\overline{S_iS_j}$	directed flux area	m^2
$k_{g,n}$	grey gas absorption coefficient	$m^{-1}atm^{-1}$
K_d	derivative gain	-
K_i	integral gain	-
K_p	proportional gain	-
P_b	proportional band	°C
$\dot{q}_{conv}$	heat flux to a surface zone by convection	W m^{-2}
$\dot{Q}_a$	heat release from air	W
$\dot{Q}_{conv}$	heat convection	W
$\dot{Q}_{enth}$	enthalpy transport term	W
$\dot{Q}_{fuel,net,i}$	heat input of fuel	W
$\dot{Q}_s$	net heat received by surface zone	W
$\dot{Q}_{wc}$	heat losses through the water-cooling	W
t	time	s
T_g	temperature of gas zone	°C
T_s	temperature of surface zone	°C
T_{sp}	set-point temperature	°C
u	output of PID controller	°C
v	normalised output	-
V	volume of gas zone	°C
σ	Stefan-Boltzmann constant (5.6687×10^{-8})	W m^{-2} K^{-4}
ε	emissivity	-

Appendix

The measured and predicted temperatures of the selected areas in Celsius degree (°C)

Tag	Measurement			Prediction	Difference [1]		
	Max.	Avg.	Min.		Max.	Avg.	Min.
Area 1	1311.5	1292.2	1275.5	1255.7	4.25	2.82	1.55
Area 2	1239.4	1224.1	1195.4	1243.3	-0.31	-1.57	-4.01
Area 3	1251.5	1236.8	1191.9	1236.1	1.23	0.06	-3.71
Area 4	1251.1	1240.7	1213.6	1236.4	1.17	0.35	-1.88
Area 5	1250.8	1242.3	1218.7	1239.7	0.89	0.21	-1.72
Area 6	1252.5	1242.2	1219.7	1240.9	0.93	0.10	-1.74
Area 7	1248.9	1243.2	1234.7	1247.1	0.14	-0.31	-1.00
Area 8	1283.0	1262.9	1244.4	1252.7	2.36	0.81	-0.67
Area 9	1282.4	1252.0	1157.1	1256.8	2.00	-0.38	-8.62
Area 10	1265.6	1246.9	1204.9	1254.4	0.88	-0.60	-4.11
Area 11	1273.3	1255.9	1245.2	1260.1	1.04	-0.33	-1.20
Area 12	1263.9	1253.6	1238.0	1252.3	0.92	0.10	-1.16
Area 13	1252.0	1220.2	1166.4	1267.8	-1.26	-3.90	-8.69
Area 14	1251.1	1228.9	1183.9	1253.9	-0.22	-2.03	-5.91
BloomC		1249.3		1257.0		-0.62	
BloomL		1264.7		1260.0		0.37	
BloomR		1244.1		1251.7		-0.61	

RoofL	1265.3	1252.9	0.98
RoofR	1254.5	1260.1	-0.45
Z5T/C-C	1252.9	1252.7	0.02
Z5T/C-R	1250.0	1256.8	-0.54

[1] $Difference = \frac{Measure. - Predict.}{Measure.} \times 100\%$, (Measure. : Max., Avg., Max.)

391
392
393 **References**

394 [1] Y. Yang, Y. Lu, Dynamic model based optimization control for reheating furnaces, Comput.
395 Ind. 10 (1988) 11–20. doi:10.1016/0166-3615(88)90044-9.
396 [2] R. Prieler, B. Mayr, M. Demuth, B. Holleis, C. Hochenauer, Numerical analysis of the
397 transient heating of steel billets and the combustion process under air-fired and oxygen
398 enriched conditions, Appl. Therm. Eng. 103 (2016) 252–263.
399 doi:10.1016/j.applthermaleng.2016.04.091.
400 [3] R. Prieler, B. Mayr, M. Demuth, B. Holleis, C. Hochenauer, Prediction of the heating
401 characteristic of billets in a walking hearth type reheating furnace using CFD, Int. J. Heat Mass
402 Transf. 92 (2016) 675–688. doi:10.1016/j.ijheatmasstransfer.2015.08.056.
403 [4] J.M. Casal, J. Porteiro, J.L. Míguez, A. Vázquez, New methodology for CFD three-
404 dimensional simulation of a walking beam type reheating furnace in steady state, Appl. Therm.
405 Eng. 86 (2015) 69–80. doi:10.1016/j.applthermaleng.2015.04.020.
406 [5] B. Mayr, R. Prieler, M. Demuth, L. Moderer, C. Hochenauer, CFD analysis of a pusher type
407 reheating furnace and the billet heating characteristic, Appl. Therm. Eng. 115 (2017) 986–994.
408 doi:10.1016/j.applthermaleng.2017.01.028.
409 [6] Y. Yang, Y. Lu, Development of a computer control model for slab reheating furnaces,
410 Comput. Ind. 7 (1986) 145–154. doi:10.1016/0166-3615(86)90036-9.
411 [7] E. E. Madsen, STEELTEMP - A program for temperature analysis in steel plants, J. Mater.
412 Process. Tech. 42 (1994) 187–195. doi:10.1016/0924-0136(94)90138-4.
413 [8] A. Jaklič, F. Vode, T. Kolenko, Online simulation model of the slab-reheating process in a
414 pusher-type furnace, Appl. Therm. Eng. 27 (2007) 1105–1114.
415 doi:10.1016/j.applthermaleng.2006.07.033.
416 [9] A. Steinboeck, D. Wild, T. Kiefer, A. Kugi, A mathematical model of a slab reheating furnace
417 with radiative heat transfer and non-participating gaseous media, Int. J. Heat Mass Transf. 53
418 (2010) 5933–5946. doi:10.1016/j.ijheatmasstransfer.2010.07.029.
419 [10] J.Y. Jang, J.B. Huang, Optimization of a slab heating pattern for minimum energy
420 consumption in a walking-beam type reheating furnace, Appl. Therm. Eng. 85 (2015) 313–321.
421 doi:10.1016/j.applthermaleng.2015.04.029.
422 [11] Y. Il Kim, K.C. Moon, B.S. Kang, C. Han, K.S. Chang, Application of neural network to the
423 supervisory control of a reheating furnace in the steel industry, Control Eng. Pract. 6 (1998).
424 doi:10.1016/S0967-0661(98)00098-7.
425 [12] P. Laurinen, J. Röning, An adaptive neural network model for predicting the post roughing
426 mill temperature of steel slabs in the reheating furnace, J. Mater. Process. Technol. 168 (2005)
427 423–430. doi:10.1016/j.jmatprotec.2004.12.002.
428 [13] Y. Liao, M. Wu, J.-H. She, Modeling of reheating-furnace dynamics using neural network

based on improved sequential-learning algorithm, in: 2006 IEEE Int. Conf. Control Appl., Munich, Germany, 4-6 October, 2006: pp. 3175–3181. doi:10.1109/CACSD-CCA-ISIC.2006.4777146.

[14] H.C. Hottel, A.F. Sarofim, Radiative transfer, New York: McGraw-Hill, 1967.

[15] L. Shen, J. He, C. Yang, W. Gui, Multi-zone multi-phase temperature field modelling of aluminum alloy workpieces in large-scale vertical quench furnaces, Appl. Therm. Eng. 113 (2017) 1569–1584. doi:10.1016/j.applthermaleng.2016.11.058.

[16] A. Emadi, A. Saboonchi, M. Taheri, S. Hassanpour, Heating characteristics of billet in a walking hearth type reheating furnace, Appl. Therm. Eng. 63 (2014) 396–405. doi:10.1016/j.applthermaleng.2013.11.003.

[17] C.K. Tan, J. Jenkins, J. Ward, J. Broughton, A. Heeley, Zone modelling of the thermal performances of a large-scale bloom reheating furnace, Appl. Therm. Eng. 50 (2013) 1111–1118. doi:10.1016/j.applthermaleng.2012.06.046.

[18] Y. Hu, J. Niska, J. Broughton, E. McGee, C. Tan, A. Matthew, P. Roach, Zone modelling coupled with dynamic flow pattern for the prediction of transient performance of metal reheating, in: AISTech2014-The Iron Steel Technol. Conf. Expo., Indianapolis, USA, 5-8 May, 2014.

[19] Y. Hu, C.K. Tan, J. Broughton, P.A. Roach, Development of a first-principles hybrid model for large-scale reheating furnaces, Appl. Energy. 173 (2016) 555–566. doi:10.1016/j.apenergy.2016.04.011.

[20] Y. Hu, C. Tan, J. Broughton, P. Roach, L. Varga, Model-based multi-objective optimisation of reheating furnace operations using genetic algorithm, in: 9th Int. Conf. Appl. Energy, Cardiff, UK, 21-24 August, 2017.

[21] W. Boyes, Instrumentation Reference Book, 4th ed., USA: Butterworth-Heinemann, 2009.

[22] A.D. Matthew, C.K. Tan, P.A. Roach, J. Ward, J. Broughton, A. Heeley, Calculation of the radiative heat-exchange areas in a large-scale furnace with the use of the monte carlo method, J. Eng. Phys. Thermophys. 87 (2014) 732–742. doi:10.1007/s10891-014-1067-4.

[23] J.M. Rhine, R.J. Tucker, Modelling of gas-fired furnaces and boilers: And Other Industrial Heating Processes, New York: McGraw-Hill Inc, 1991.

[24] F. Hildebrand, Introduction to numerical analysis, Dover Publications, 1987.

[25] G.R. Hurd, J. Kaufman, H.C. Wu, J. Ward, E. Rodriguez, Process control and automation systems advancements for reheat furnaces, Iron Steel Technol. 8 (2011) 67–74.